Supplement of Atmos. Chem. Phys., 23, 3453–3470, 2023
https://doi.org/10.5194/acp-23-3453-2023-supplement

Atmospheric Chemistry and Physics
Open Access
EGU

Supplement of

Boundary layer moisture variability at the Atmospheric Radiation Measurement (ARM) Eastern North Atlantic observatory during marine conditions

Maria P. Cadeddu et al.

Correspondence to: Maria P. Cadeddu (mcadeddu@anl.gov)

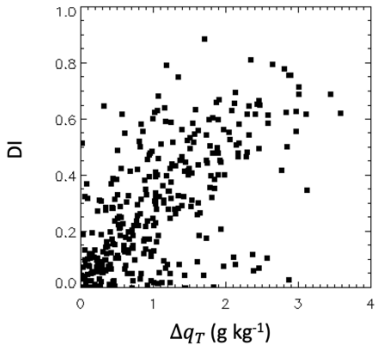

Figure S1: Scatterplot of the index from Jones et al., 2011 (x-axis) and the index from Sena et al. (2016) used in the present paper (y-axis), N=334 cases.

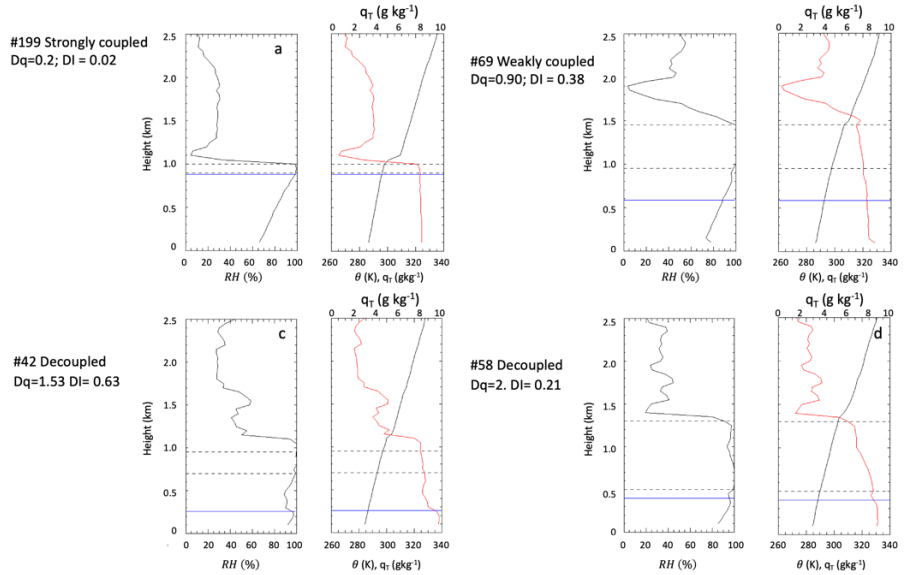

Figure S2: First and 3rd column: Relative humidity. Second and 4th column: Total water mixing ratio (red, top axis) and potential temperature (black). Dashed lines are the cloud base and cloud top height, and the blue line is the LCL. The four panels show (a) coupled, weakly decoupled (b), and decoupled (c) cases. In Fig. 1d is shown one case in which the 2 indexes don't agree (about 12% of the cases). Note that in all these cases the potential temperatures are weakly stable in the sub-cloud layer. According to the 2 indexes about 60% of cases are weakly decoupled ($\Delta q_T < 1.3$).

	$\frac{\partial \hat{h}}{\partial t}$	$\boldsymbol{v} \cdot \boldsymbol{\nabla} \hat{h}$	ω_s	ω_e
Jan	1.5±2.7	-0.7±2.5	-3.4 ± 2.2	4.1 ± 4.2
Feb	1.2±3.2	-1.4±2.2	-3.4 ± 1.9	3.2± 4.4
Mar	0.9±3.5	-0.8±2.2	-3.6 ± 2.0	3.7 ± 4.6
Apr	0.1±3.4	-0.9±2.2	-3.2 ± 1.9	2.4 ± 4.6
May	0.1±3.8	-1.0±2.4	-3.5 ± 1.9	2.6 ± 4.9
Jun	0.4±3.6	-0.8±2.1	-2.8 ± 1.8	2.5 ± 4.4
Jul	0.2±3.2	-0.7±1.9	-2.2 ± 1.7	1.7 ± 4.0
Aug	0.4±3.5	-1.3±2.1	-2.7 ± 1.8	1.8 ± 4.4
Sep	0.4±3.7	-1.1±2.3	-3.5 ± 1.9	2.7 ± 4.8
Oct	0.7±3.4	-1.1±2.2	-3.5 ± 1.9	3.1 ± 4.6
Nov	0.7±3.4	-1.2±2.2	-3.4 ± 2.0	2.9 ± 4.5
Dec	0.4±3.5	-1.4±2.3	-3.2 ± 1.9	2.2 ± 4.7

Table S1: Monthly averages and standard deviation of the components of the mass budget in (3). All values are reported here in mm s^{-1}.

Date	Ts (K)	Ps (mb)	qs (g kg^{-1})	C_{base} (km)	C_{top} (km)	rr@CB (mm day^{-1})	PWV (cm)	LWP (g m^{-2})	Ws@cb m s^{-1}
2017/03/16	286.5±0.3	1028.6±0.5	5.5±0.1	1.4±0.2	1.7±0.2	2.2±5.8	1.2±0.1	35.9±81.0	9.0±0.6
2017/03/17	286.4±0.3	1028.6±0.5	5.7±0.2	1.4±0.1	1.6±0.1	0.±1.3	1.3± 0.1	65.8±65.1	8.2±1.0
2018/08/05	295.1±0.3	1020.7±0.9	11.1±0.8	1.0±0.1	1.3±0.1	0.8 ±1.3	3.1± 0.1	100.1±78.5	4.5±0.5
2018/09/04	294.5±0.2	1020.1±0.1	9.7±0.7	1.3±0.3	1.9±0.3	4.2±5.5	2.4± 0.1	112.4±151.6	5.5±1.2
2019/03/31	286.5±0.3	1019.5±0.1	5.5±0.2	1.4±0.3	1.8±0.3	1.6±2.9	1.1± 0.1	119.7±88.4	5.9±1.8
2019/04/04	286.3±0.3	1022.0±1.1	5.6±0.2	1.2±2.6	1.7±0.4	1.6±3.3	1.2± 0.1	97.2±90.8	11.0±1.5
2019/06/04	290.0±0.2	1024.1±0.8	7.8±0.2	1.4±0.3	1.7±0.2	1.8±4.2	1.9± 0.1	51.0±91.3	7.8±1.6
2019/06/08	290.6± 0.1	1023.2±1.3	9.5±0.4	0.8±0.5	0.9±0.1	0.1±0.1	3.0±0.2	33.6±40.2	5.1±2.7
2019/06/25	291.9 ±0.2	1020.1±1.2	9.4±0.6	1.2±0.2	1.5±0.2	0.3±0.7	2.0±0.1	45.4±62.6	6.3±0.9
2019/06/26	291.8± 0.2	1023.1±0.4	9.5±0.4	1.4±0.3	1.7±0.3	4.2±13.3	2.2±0.1	48.6±102.1	8.3±0.7

Table S2: List of cases used in Section 5, and daily mean values of surface temperature, surface pressure, surface mixing ratio, cloud base height, cloud top height, rain rate at cloud base, precipitable water vapor, liquid water path, wind speed at cloud base.

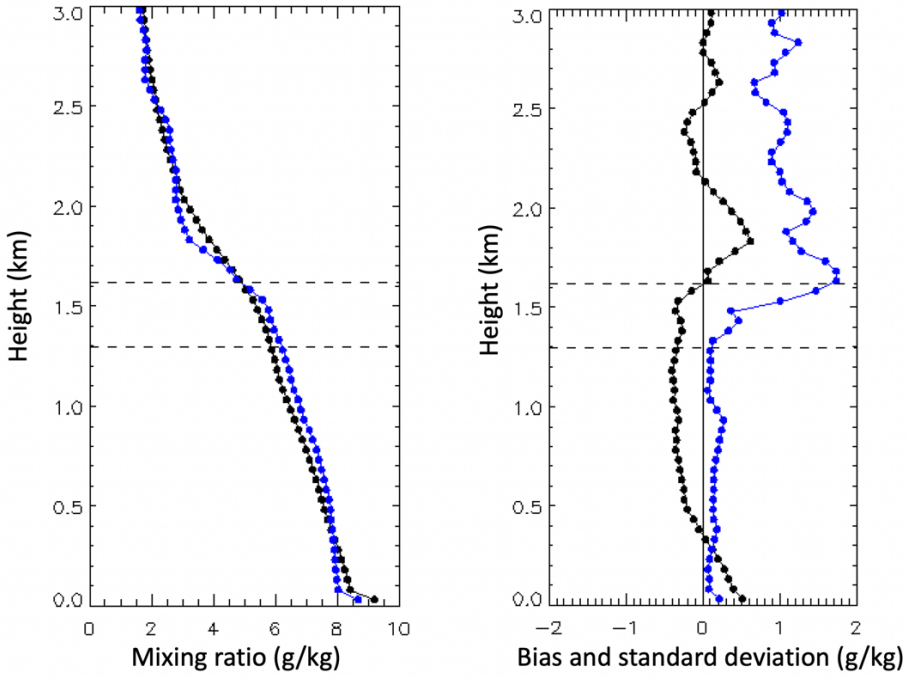

Figure S3: Average profile of mixing ratio from radiosondes (blue) and Raman lidar (black). (b) Bias (black) and standard deviation (blue) of the differences between retrieved and radiosondes mixing ratio. The horizontal dashed lines indicate average cloud base and cloud top during the selected cases.